Supplementary Materials For: A single-cell biochemistry approach reveals PAR complex dynamics during cell polarization

Daniel J. Dickinson[1,2], Francoise Schwager[3], Lionel Pintard[4], Monica Gotta[3] and Bob Goldstein[1]

[1] Department of Biology and Lineberger Comprehensive Cancer Center, University of North Carolina at Chapel Hill, Chapel Hill, NC 27599

[2] Present address: Department of Molecular Biosciences, University of Texas, Austin, TX 78712

[3] Department of Cell Physiology and Metabolism, University of Geneva Medical Faculty, 1, rue Michel Servet, 1211 Geneva, Switzerland

[4] Institut Jacques Monod, Cell Cycle and Development Team, Centre National de la Recherche Scientifique and University of Paris Diderot and Sorbonne Paris Cité UMR7592, Paris 75013, France

Corresponding Author / Lead Contact:
Daniel J. Dickinson
Department of Molecular Biosciences
NHB 2.606, Stop A5000, 100 East 24th St.
Austin, TX 78712
650-815-1923
daniel.dickinson@austin.utexas.edu

Dickinson et al. Figure S1

A

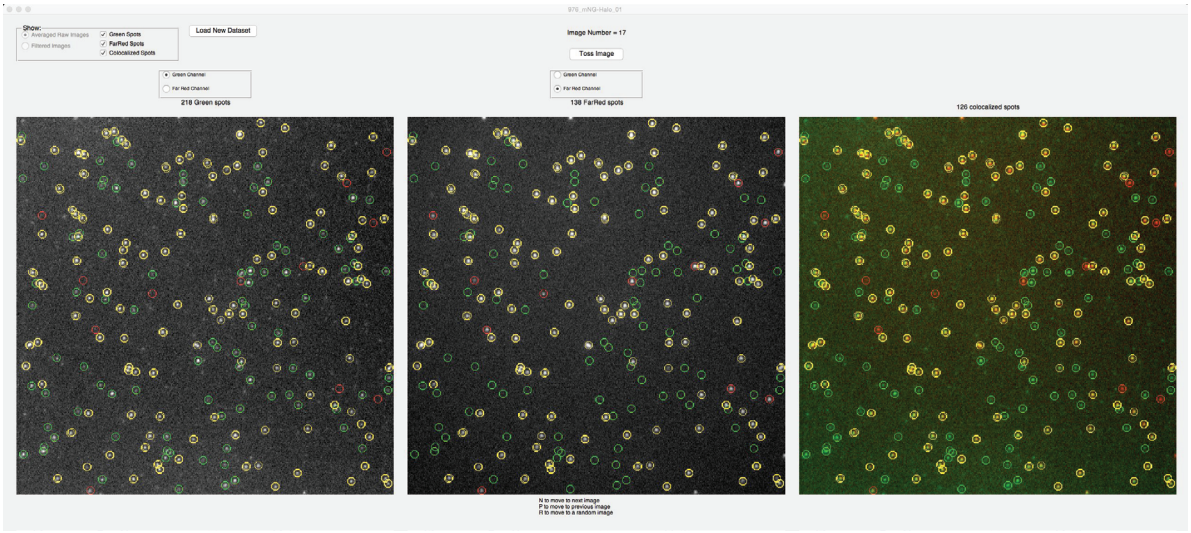

B

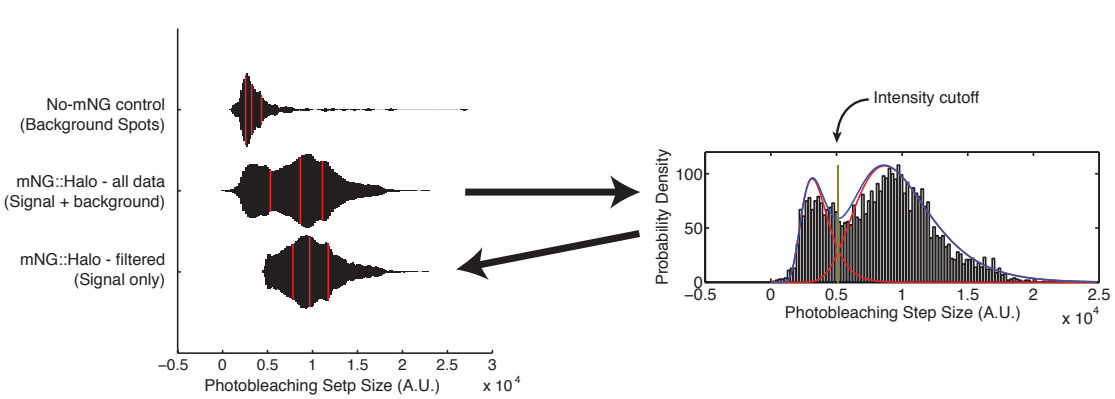

C

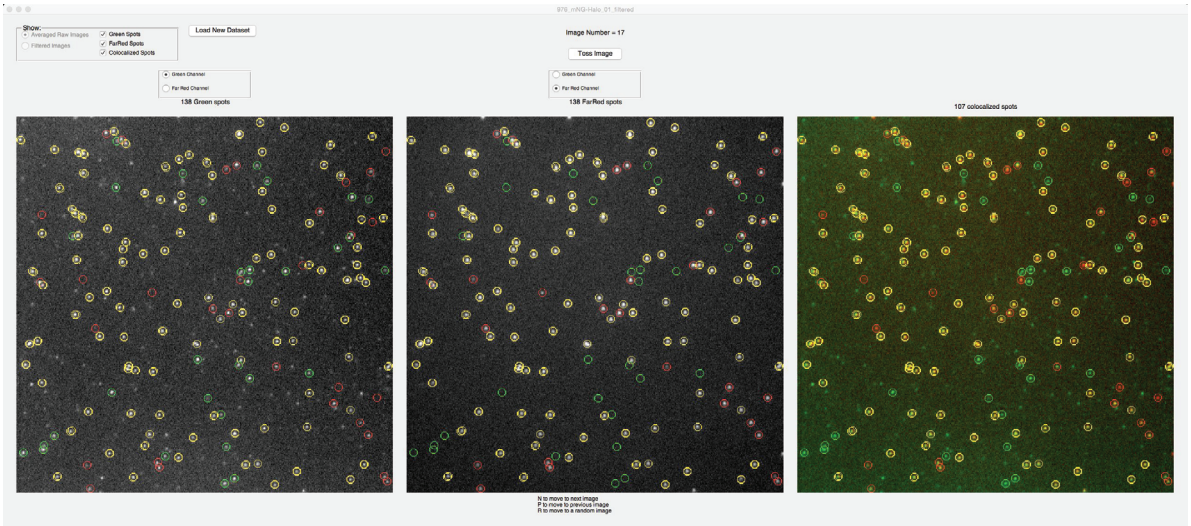

Figure S1, related to Figure 1 and Methods: Automated spot detection

A. Screen shot from our software showing the results of image segmentation. The three image panels show the green channel (left), far-red channel (center) and merged image (right). Green spots found by the software are highlighted with green circles, far-red spots with red circles, and colocalizing spots with yellow circles.

B. Illustration of the filtering routine that we adopted in order to remove dim background spots that were present in the green channel. The left panel shows the distributions of molecular fluorescence intensities (i.e., photobleaching step sizes) in the green channel for a sample with no mNG (top), an mNG::HaloTag sample before filtering (middle) and after filtering (bottom). The unfiltered data comprises two intensity distributions: a dim background population that is also present in the sample with no mNG present, and a brighter population that we infer corresponds to bona fide mNG molecules. To eliminate the dim spots, we fit the distribution of step sizes to the sum of two log-normal distributions as shown in the right panel. An intensity cutoff was defined by the local minimum between the two log-normal peaks, which is a compromise that eliminates as much background as possible without sacrificing too much signal. Photobleaching steps smaller than this magnitude were removed from the data, and spots that had no remaining photobleaching steps after applying this step size filter were ignored.

C. Screen shot of the same data as in (A) after applying the intensity filter.

Dickinson et al. Figure S2

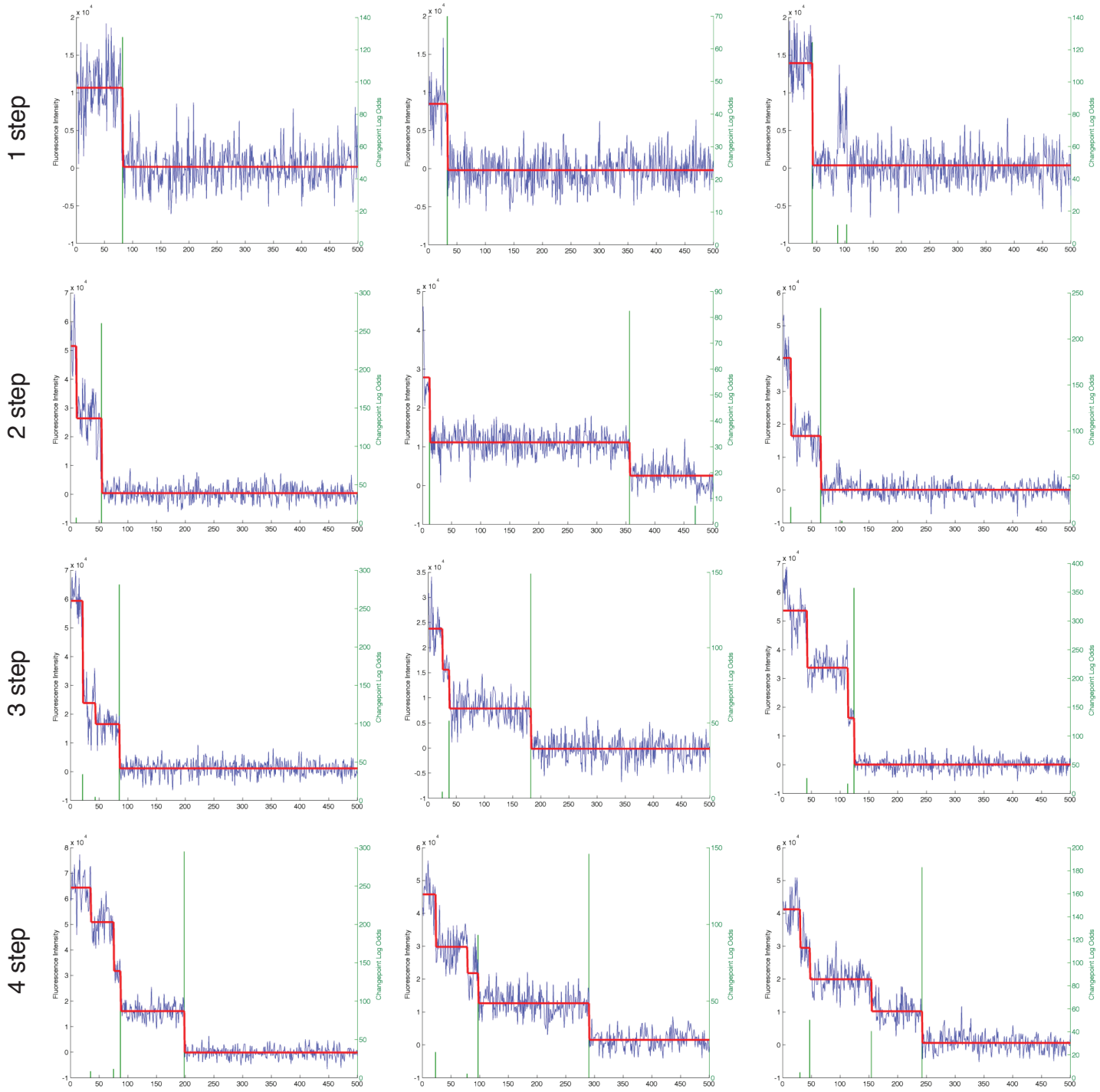

Figure S2, related to Figure 1 and Methods: Automated detection and counting of photobleaching steps

Shown is a gallery of examples randomly selected (using a random number generator) from an mNG::AraD dataset. The blue traces show the raw single-molecule intensity data, and the red traces show the photobleaching steps identified by our software. The green bars show the statistical confidence with which each step was detected, expressed as a log odds ratio. Steps with a log odds ratio greater than 2 (i.e., 99% confidence) were considered to be bona fide photobleaching steps unless eliminated by the intensity filter illustrated in Figure S1. Visible photobleaching steps were generally identified with vastly greater confidence than this conservative threshold.

Dickinson et al. Figure S3

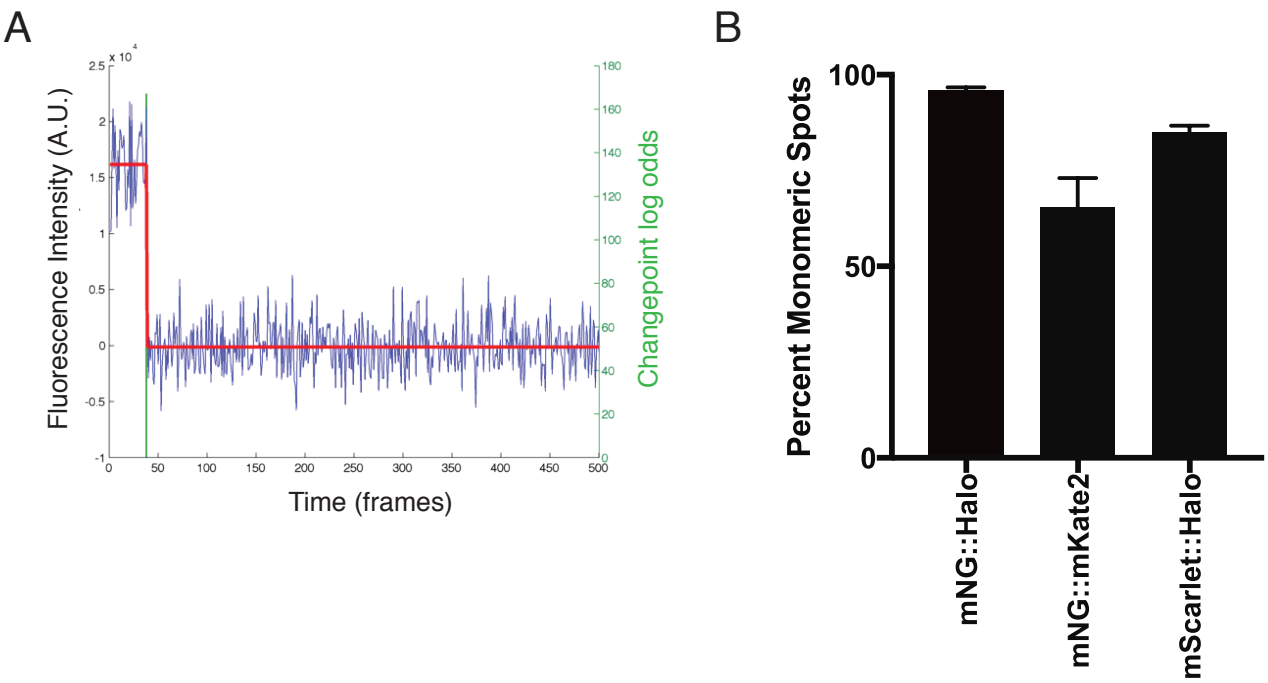

Figure S3, related to Figure 1: Single-step photobleaching of mNG::HaloTag molecules and aggregation tendency of mNG::mKate2

A. Example of a single-step photobleaching trace for an mNG::HaloTag molecule. This trace was selected at random from an mNG::HaloTag dataset.

B. Fraction of monomeric steps observed with mNG::HaloTag, mNG::mKate2 and mScarlet-I::HaloTag. 95.8% ± 0.9% of mNG::HaloTag molecules were found to be monomeric; the remaining 4.2% of cases most likely represent pairs of mNG::HaloTag molecules that bound the coverslip within the limit of optical resolution by chance. In contrast, mNG::mKate2 (65.3 ± 7.7% monomeric) and to a lesser extent mScarlet-I::HaloTag (85.1 ± 1.6% monomeric) have a tendency to oligomerize. n = 24,895 spots counted from 7 embryos for mNG::HaloTag, n = 33,409 spots counted from 13 embryos for mNG::mKate2 and n=23,181 spots counted from 11 embryos for mScarlet-I::HaloTag.

Dickinson et al. Figure S4

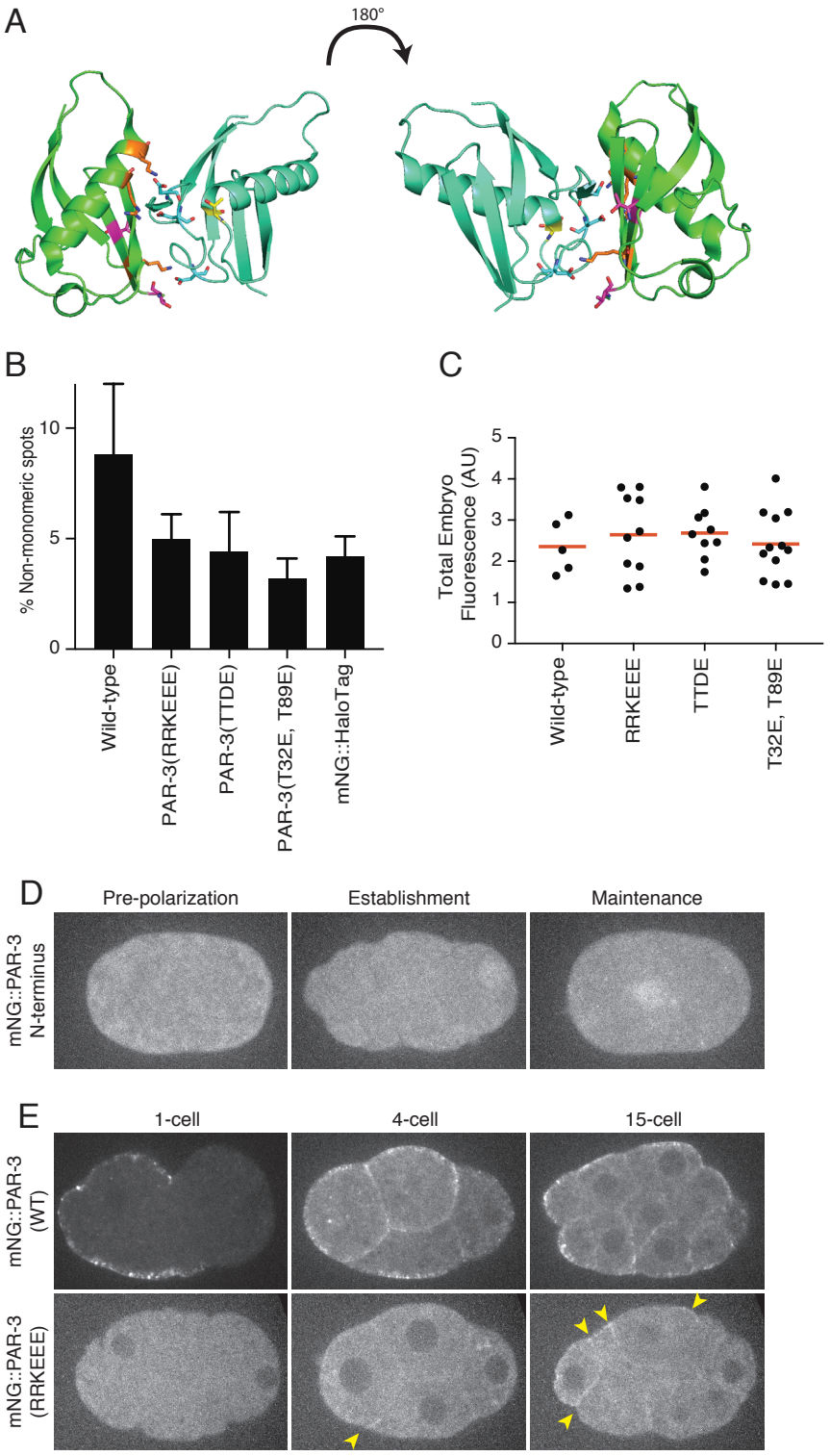

Figure S4, related to Figures 5, 6 and 7: Oligomerization-blocking mutations in PAR-3

A. Model of the PAR-3 N-terminal domain based on a published crystal structure of mammalian PAR-3 (Zhang et al., 2013). Three basic residues, shown in orange, form salt bridges with acidic residues (cyan) that stabilize the dimerization interface. These residues were mutated to glutamic acid to create the RRKEEE mutant. Two threonine residues that pack at the dimerization interface, shown in pink, were mutated to acidic residues to create the TTDE mutant. T89, which is phosphorylated by PLK-1, is shown in yellow.

B. B) Fraction of non-monomeric spots observed when the indicated proteins were pulled down. The PAR-3 mutants are not measurably different from the monomeric mNG::HaloTag control protein. These same data are plotted as a distributions of oligomer sizes in Figures 5B and 7D.

C. Quantification of protein expression levels of wild-type and monomeric mutant mNG::PAR-3 in 1-cell embryos. The oligomerization-blocking mutants do not affect PAR-3 protein levels.

D. Localization of the N-terminus of PAR-3 (amino acid residues 1-184) expressed alone, in the absence of wild-type PAR-3. No visible membrane localization is observed.

E. Localization of PAR-3(WT) and PAR-3(RRKEEE) at later developmental stages. Although PAR-3(RRKEEE) does not bind stably to the plasma membrane at the 1-cell stage, it can localize weakly to the plasma membrane at later stages.

Dickinson et al. Figure S5

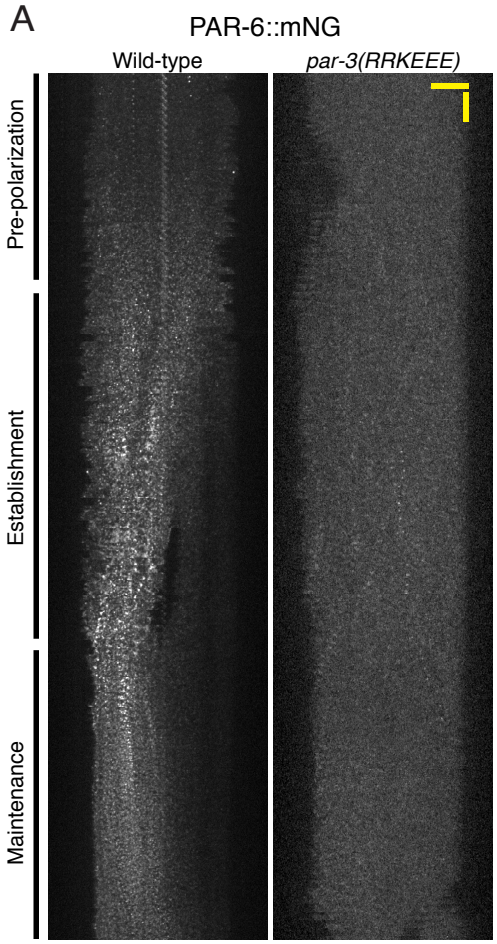

B

Strain	% Embryonic Lethality (n)	% Sterile Adults (n)
Wild-type	0% (307)	0.3% (357)
mNG::PAR-3 (WT)	0% (249)	0% (319)
mNG::PAR-3 (RRKEEE)	40% (481)	72% (200)
mNG::PAR-3 (TTDE)	21% (408)	32% (329)
mNG::PAR-3 (T32E, T89E)	4.3% (531)	16.1% (589)
Halo::PAR-3 (WT)	0% (380)	0% (488)
Halo::PAR-3 (RRKEEE)	28% (124)	49% (100)

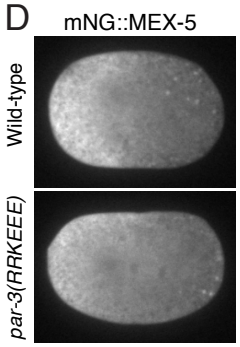

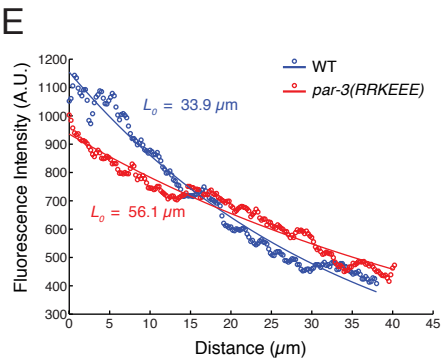

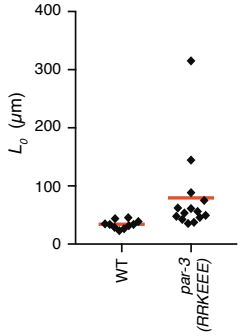

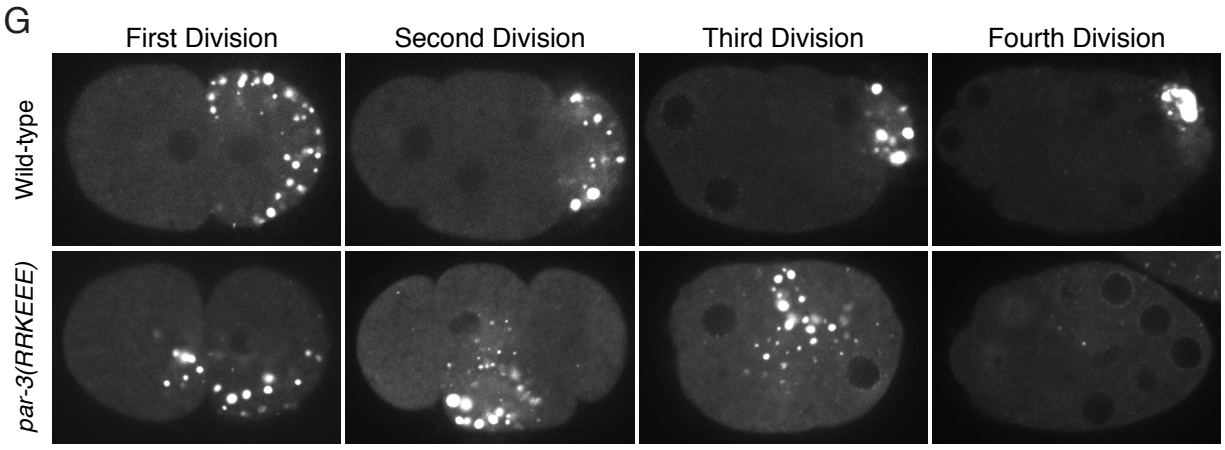

Figure S5, related to Figures 5 and 7: Polarity phenotypes in *par-3(RRKEEE)* mutants

A. Kymographs of cortical PAR-6::mNG in wild-type and *par-3(RRKEEE)* mutant zygotes. Anterior is to the left. Horizontal scale bar represents 10 μm and vertical scale bar represents 1 min.
B. Scoring of embryonic lethality and adult sterility in the indicated strains.
C. Examples of the localization of endogenously tagged mNG::MEX-5 during maintenance phase in wild-type and *par-3(RRKEEE)* mutant embryos. The two examples shown were chosen because they had gradient lengths as close as possible to the mean of each population.
D. To quantify MEX-5 localization, we measured fluorescence intensity as a function of distance along the AP axis. We then fit each intensity profile to the exponential decay function $I = Ae^{-\ell/L_0}$ to extract the characteristic gradient decay length L_0. A larger value of L_0 indicates a shallower gradient. Shown here are quantification and fits for the two embryos shown in (C).
E. Distribution of MEX-5 gradient lengths L_0 in wild-type and *par-3(RRKEEE)* mutant embryos.
F. Examples of P granule segregation defects in *par-3(RRKEEE)* mutant embryos. P granules were visualized in live embryos using a GFP::PGL-1 transgene (Cheeks et al., 2004). We observed mis-segregation of P granules at each germ cell division, and P granules were often lost entirely by the 16-cell stage. See Table S1 for a complete description of all phenotypes observed.

Dickinson et al. Figure S6

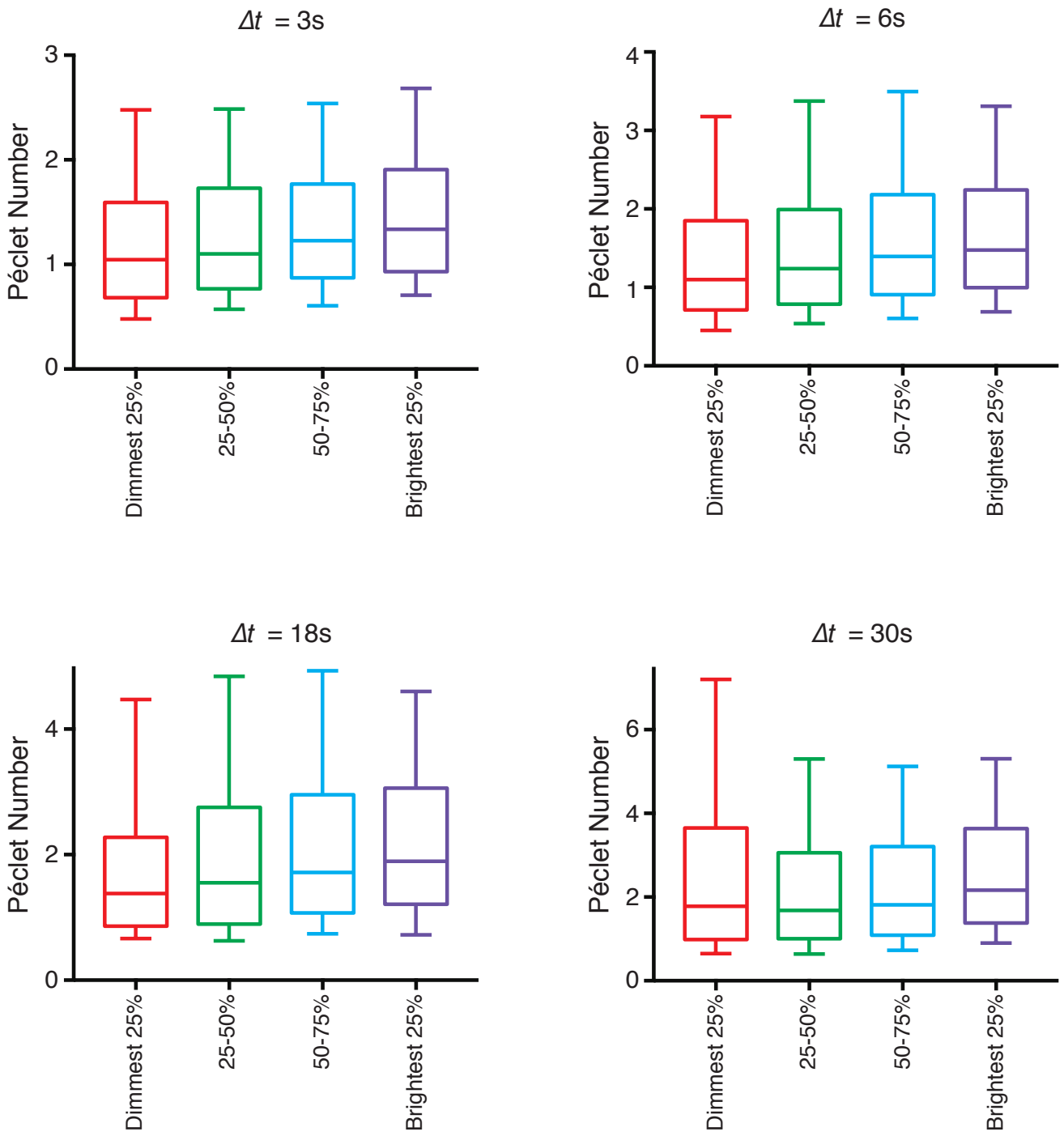

Figure S6, related to Figure 6: Trend towards increasing Péclet number for larger PAR-3 particles is independent of the choice of time step
Shown are distributions of the Péclet number (the ratio of advective to diffusive transport rates) for PAR-3 particles of different intensities, calculated using different time steps (see Methods). For each plot, the whiskers show the 10th and 90th percentiles, and the center line shows the median. The value of the Péclet number increases with increasing Δt , as expected, but the trend is the same regardless of the value chosen. The plot with Δt = 3 is shown in the main text (Figure 7H).

Dickinson et al. Figure S7

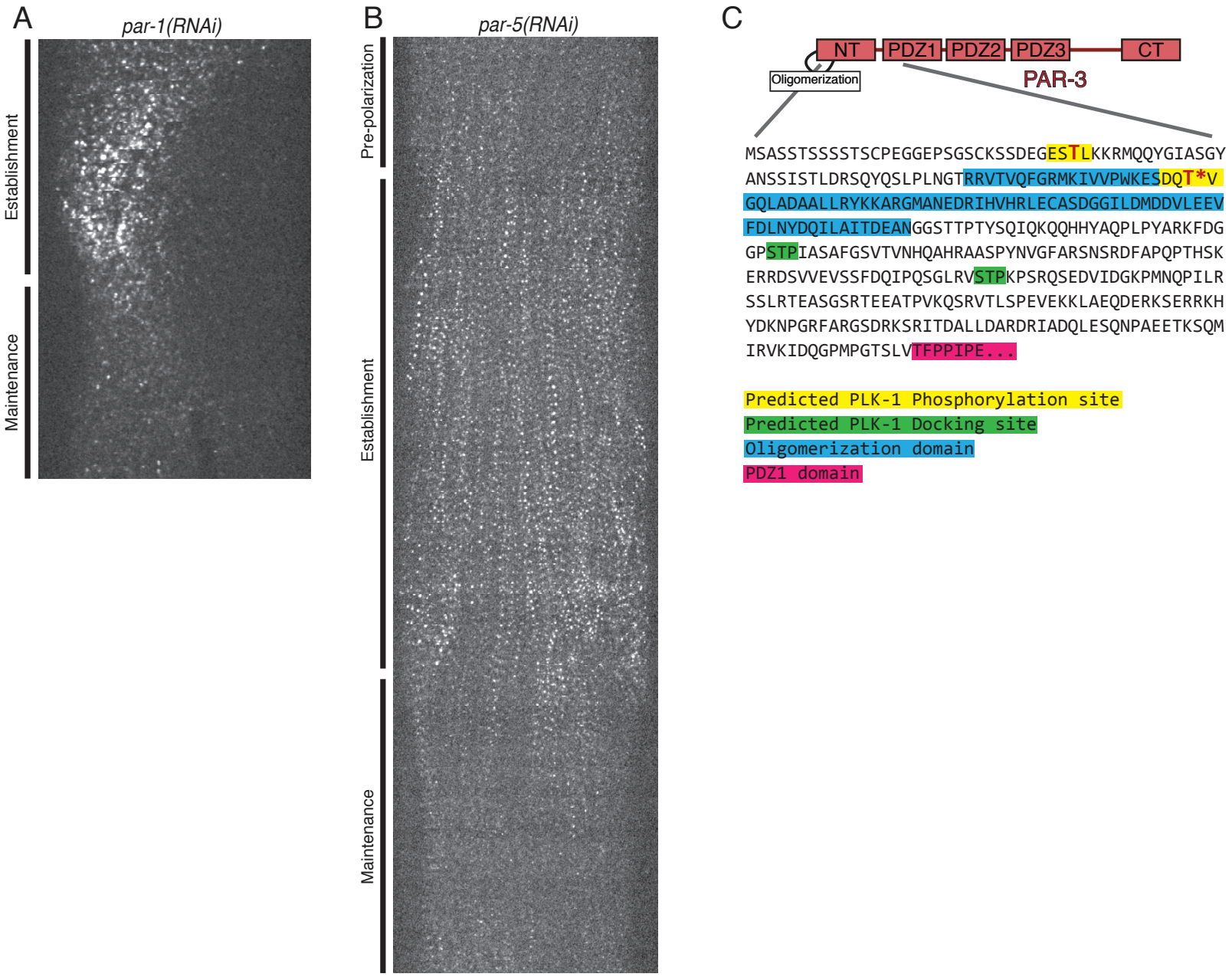

Figure S7, related to Figure 7: Regulation of PAR-3 oligomerization

A.B. Kymographs of cortical mNG::PAR-3 in (A) par-1(RNAi) or (B) par-5(RNAi) embryos. Anterior is to the left.

C. PLK-1 phosphorylation sites in PAR-3. Predicted phosphorylation sites at the N-terminus of PAR-3 were identified using ELM (Dinkel et al., 2016). Threonine 89 (labeled with an asterisk in the second PLK consensus site) was identified as phosphorylated via mass spectrometry (see Methods).

Dickinson et al. Figure S8

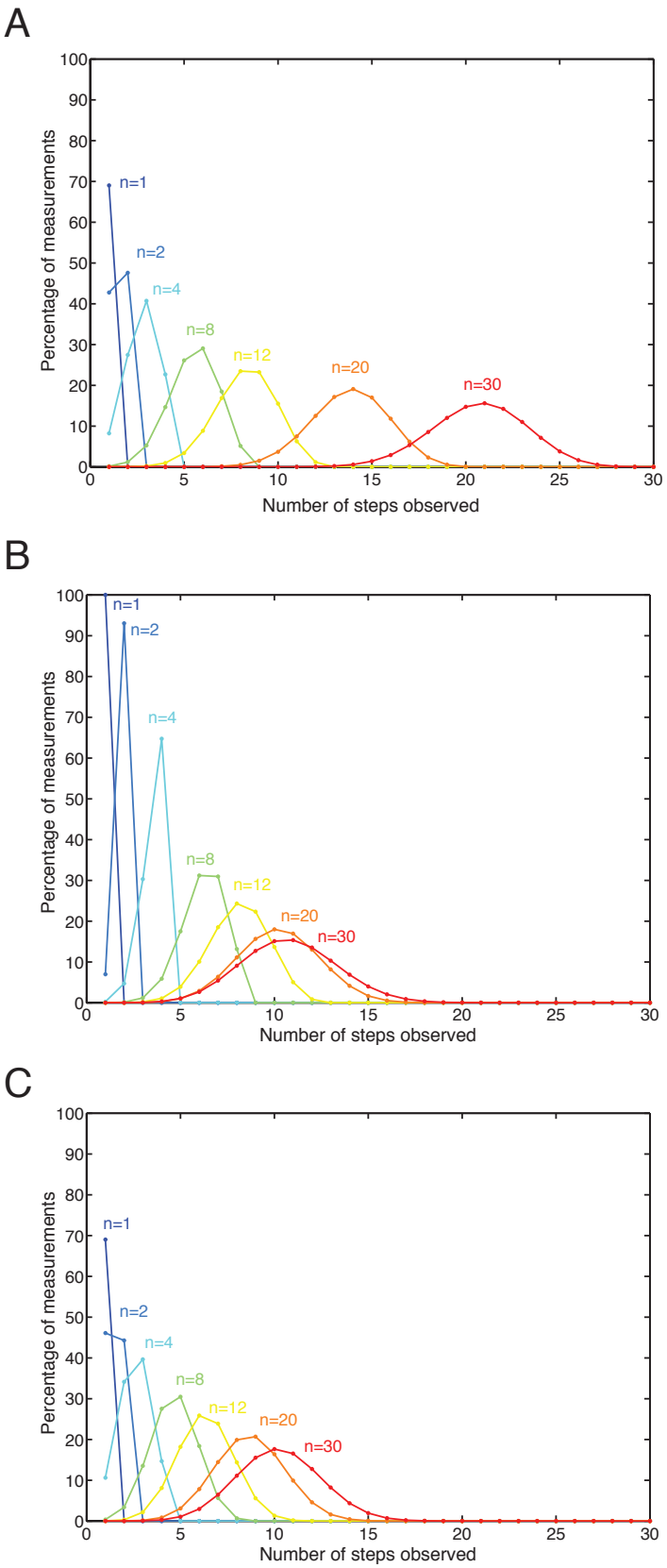

Figure S8, related to Methods: Impact of incomplete fluorophore maturation and simultaneous bleaching events on stoichiometry measurements

A. Effect of incomplete fluorophore detection on observed step counts. Each curve shows the expected distribution of measured complex sizes for a pure population of oligomers of the indicated sizes, given the detection efficiency d = 0.69 measured in our experiments for mNG.

B. Effect of simultaneous photobleaching events on observed step counts. Each curve shows the expected distribution of measured complex sizes for a population containing the indicated number of active fluorophores, given kbleach = 0.012 frame-1 as measured in our experiments for mNG.

C. Combined effects of simultaneous photobleaching and incomplete detection on observed step counts. Each curve shows the expected distribution of measured complex sizes for a pure population of oligomers containing the indicated number of molecules.

Dickinson et al. Table S1

Number of Embryos	Description of Phenotype
6	Apparently normal
1	P granules were inherited by both P0 daughters, then were segregated to the anterior (EMS-position) cell at the 4-cell stage and were grossly mis-positioned thereafter. P granules appeared to be lost altogether after the 16-cell stage.
1	P granules were inherited by both P0 daughters, present in multiple cells at the 8-cell stage, and then largely lost by the 15-cell stage.
1	P granules were inherited by both P0 daughters, but asymmetry was recovered at 2-cell stage and appeared normal thereafter.
1	P granules were inherited by the anterior cell (closest to the polar bodies) at first division. P granules subsequently formed in daughters of the posterior cell and were present in 3 cells at the 4-cell stage, then were grossly mis-positioned thereafter.
1	P granules were lost during the first division, then recovered in P1, then lost again during P2 division.
1	P granules were lost during the first division, then recovered in P1 but also in ABa. A grossly normal distribution was recovered by the 15-cell stage.
1	First division was normal but P granules were inherited by both P1 daughters.
1	First division was normal but P granules were inherited by both P1 daughters. Normal P granule positioning was recovered at 4-cell stage; then, P granules were inherited by the wrong daughter of P3 (what should have been the D cell).
1	First division was normal but P granules were inherited by the wrong daughter of P1 (what should have been the EMS cell).
1	First division was normal but P granules were lost during the second division, then recovered in the 2 middle cells at the 4-cell stage and clearly in wrong cell at the 8-cell stage.
1	First two divisions were normal but P granules were inherited by both P2 daughters. P granules were present in multiple cells by the 15-cell stage.
1	First two divisions were normal but P granules were inherited by both P2 daughters. P granules were present in a single cell by the 15-cell stage but it was unclear if it was the correct cell.
3	First two divisions were normal but P granules were inherited by both P2 daughters. Asymmetry subsequently recovered and the 15-cell stage appeared normal.
1	First two divisions appeared largely normal although this embryo had gross defects in cell positioning. P granules were inherited by the anterior daughter of P2.
1	First two divisions were normal but P granules were inherited by the wrong P2 daughter (what should have been the C cell). P granules were largely lost by the 15-cell stage.
1	First two divisions were normal but P granules were lost during P2 division, then appeared to form and dissolve again in multiple cells during the 8-15 cell stages.
1	P granules were absent until 8-cell stage, then appeared in the wrong cell and were inherited by both daughters when that cell divided.

Table S1, related to Figure 5: Description of P-granule phenotypes observed in *par-3(RRKEEE)* mutants
Each row describes an observed embryonic phenotype and lists the number of embryos for which that phenotype was observed.